ARTICLE

Aligned ZnO/CdTe Core−Shell Nanocable Arrays on Indium Tin Oxide: Synthesis and Photoelectrochemical Properties

Xina Wang,[†,‡] Haojun Zhu,[†] Yeming Xu,[†] Hao Wang,[‡,*] Yin Tao,[†] Suikong Hark,[†] Xudong Xiao,[†] and Quan Li[†,*]

[†]Department of Physics, The Chinese University of Hong Kong, Shatin, New Territory, Hong Kong, China, and [‡]Faculty of Physics and Electronic Technology, Hubei University, Wuhan 430062, China

ABSTRACT Vertically aligned ZnO/CdTe core−shell nanocable arrays-on-indium tin oxide (ITO) are fabricated by electrochemical deposition of CdTe on ZnO nanorod arrays in an electrolyte close to neutral pH. By adjusting the total charge quantity applied during deposition, the CdTe shell thickness can be tuned from several tens to hundreds of nanometers. The CdTe shell, which has a zinc-blende structure, is very dense and uniform both radially and along the axial direction of the nanocables, and forms an intact interface with the wurtzite ZnO nanorod core. The absorption of the CdTe shell above its band gap (~1.5 eV) and the type II band alignment between the CdTe shell and the ZnO core, respectively, demonstrated by absorption and photoluminescence measurements, make a nanocable array-on-ITO architecture a promising photoelectrode with excellent photovoltaic properties for solar energy applications. A photocurrent density of ~5.9 mA/cm^2 has been obtained under visible light illumination of 100 mW cm^{-2} with zero bias potential (*vs* saturated calomel electrode). The neutral electrodeposition method can be generally used for plating CdTe on nanostructures made of different materials, which would be of interest in various applications.

KEYWORDS: nanocable · CdTe · ZnO · photovoltaic · type II band alignment · electrodeposition

Inspired by the high-efficiency of dye-sensitized solar cells,[1] semiconductor quantum dots (QDs) such as CdS,[2,3] CdSe,[4,5] PbS,[6,7] PbSe,[8] InP,[9] and InAs[10] have recently been extensively used as light harvesters in lieu of organic dyes in the application of QD-sensitized solar cells (QDSSCs), owing to the unique size- and shape-dependent absorption properties of quantum dots.[11−14] In one of the most promising configurations of QDSSCs, the semiconductor QDs or nanocrystals are hosted on a transparent electrode, which consists of a one-dimensional (1D) ZnO and/or TiO_2 array on a conducting substrate.[15−19] In such a configuration, an appropriate band alignment between the QDs and the ZnO/TiO_2 electrode allows efficient charge carrier injection, and the single-crystal 1D nanostructures provide an ideal channel for effective carrier transport.[20−26] An incident photon-to-current efficiency (IPCE) of 50−60% has been achieved in CdSe QD-sensitized ZnO nanowire photovoltaic (PV) devices,[20] and an energy conversion efficiency of 4.15% has been realized in a CdS QD-sensitized TiO_2 nanotube solar cell.[21] Despite numerous advantages associated with QDSSCs, effective loading of QDs on the nanostructured oxide electrode[27] remains a critical problem. Although bifunctional linker molecules could improve the loading density of QDs,[20,28] they may introduce additional interface problems that hinder the injection of photogenerated electrons from QD to electrode.[29] More generally, the mitigation of interface problems in QDSSCs remains one of the most promising avenues to improved cell efficiency, as significant carrier loss can be caused by nonradiative recombination processes occurring at the interfaces between a QD and the electrolyte, the oxide electrode, and adjacent QDs.[29] Therefore, a nanocable array on a conducting substrate, and specifically a continuous semiconductor nanoshell-sensitized 1D nanoelectrode, should have improved performance as a photoelectrode over a standard QDSSC due to the improved loading density, reduced surface area of the light harvester, and greater intact interface area between the absorbing shell and the 1D oxide electrode.

Among the most widely used inorganic semiconductor sensitizers, CdTe has a high optical absorption coefficient (>10^4 cm^{-1}) and narrow band gap of ~1.5 eV,[30,31] matching the preferred range of the solar radiation spectrum. In addition, it forms a

*Address correspondence to liquan@phy.cuhk.edu.hk, wangh@hubu.edu.cn.

Received for review January 12, 2010 and accepted April 28, 2010.

Published online May 6, 2010. 10.1021/nn1001547

typical type II band alignment with ZnO,[32] allowing effective injection of photogenerated electrons from CdTe into ZnO.[25] Consequently, a ZnO/CdTe nanocable array on a transparent conductive substrate would hold great potential in a number of photoelectrical applications. Several methods may be used to deposit a semiconductor material shell on an oxide nanowire or nanotube surface: chemical base deposition (CBD), directly soaking the nanowires in well-dispersed QD solution,[21,23,25] or electrochemical deposition.[26,28] Electrochemical deposition is preferable, as it is relatively simple, scalable, and can produce a shell of reasonable density and uniformity. Unfortunately, most of the electrolytes currently used in electrodeposition of CdTe are either acidic solutions (pH 1−3) or basic solutions (pH 10) containing NH_4^+,[33−36] both of which can severely etch the ZnO. To date, a procedure for fabricating ZnO/CdTe nanocable arrays with precisely controllable properties on a conductive substrate has yet to be demonstrated.

In the present work, we demonstrate the formation of large-scale ZnO/CdTe nanocable arrays-on-indium tin oxide (ITO) through electrodeposition of CdTe on ZnO nanorod arrays in an electrolyte with close-to-neutral pH. An intact interface is formed between the single-crystal ZnO nanorod and the uniform CdTe nanoshell with tunable thickness. Good photoelectrode absorption properties and type II band alignment between the CdTe shell and the ZnO core are demonstrated by absorption and photoluminescence measurements, respectively. The resulting nanostructured photoelectrode shows good photovoltaic properties and holds promise for applications in solar energy conversion.

RESULTS AND DISCUSSION

The electrolyte proposed in this work for the electrodeposition of CdTe was an aqueous solution composed of 0.005 M potassium tellurite (K_2TeO_3), 0.05 M nitrilotriacetic acid trisodium salt (NTA, $C_6H_6NO_6Na_3$), and 0.02 M cadmium acetate with a solution pH of 8.3. To investigate the electrochemical potential of CdTe in the close-to-neutral electrolyte, a cyclic voltammetry test was performed on a pure ITO substrate. In the cyclic voltammogram of Cd^{2+} and Te^{4+}, shown in Figure 1, two cathode current peaks appear at −0.8 and −1.0 V, which respectively correspond to the reductions of TeO_3^{2-} to elemental Te and Te to Te^{2-} according to[36]

$$TeO_3^{2-} + 3H_2O + 4e \rightarrow Te^0 + 6OH^- \quad (1)$$

$$Te^0 + Cd^{2+} + 2e \rightarrow CdTe\downarrow \quad (2)$$

$$TeO_3^{2-} + Cd^{2+} + 3H_2O + 6e \rightarrow CdTe\downarrow + 6OH^- \quad (3)$$

Therefore, the deposition of CdTe on ZnO nanorod arrays was performed at a fixed potential of −1.0 V

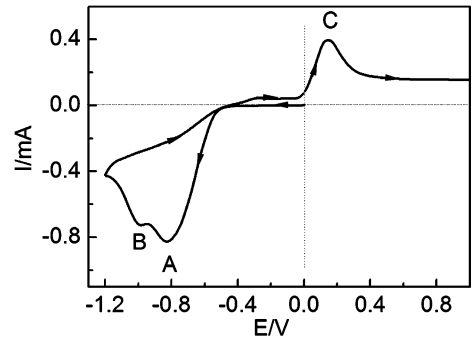

Figure 1. Cyclic voltammogram of Cd^{2+} and Te^{4+} in the neutral electrolyte on ITO electrode.

versus saturated calomel electrode (SCE) to promote the one-step reaction of TeO_3^{2-} and Cd^{2+} shown in eq 3. The thickness of the CdTe shell was adjusted by varying the total charge quantity passed through the electrodes during the electrodeposition process.

Figure 2 panels a and b show the low- and high-magnification field-emission scanning electron microscope (SEM) images of the as-grown ZnO nanorod arrays on an ITO substrate. Large-scale vertical growth of ZnO nanorod arrays has been realized. The length of the nanorods is about 7 μm, and their average diameter is 147 nm with a standard deviation of 39 nm. The nanorods have a hexagonal cross section, and the axial direction is aligned with the *c*-axis of the hexagnol ZnO crystal structure.

After electrodeposition with a total charge of 3.5 C, the ZnO nanorods were fully covered by dense CdTe nanoshells. The shell thickness is ~88 nm with a standard deviation of 10 nm. In the cross-sectional SEM image (Figure 2e), the CdTe shell is fairly homogeneous along the length of the ZnO nanowires. The energy dispersive X-ray (EDX) spectrum (Figure 2f) taken from the nanocable array after the electrodeposition reveals a Cd/Te atomic ratio close to 1 suggests that the electrochemical reaction of TeO_3^{2-} and Cd^{2+} takes place in one step, as in eq 3, without the formation of intermediate elemental Te.

Figure 3 shows the X-ray diffraction (XRD) spectra taken from pure ZnO nanorod arrays (plot a) and as-deposited (plot b) and postannealed (plot c) ZnO/CdTe nanocable arrays. For pure ZnO nanorod arrays, 10 diffraction peaks marked by asterisks can be respectively indexed to the (100), (002), (101), (102), (110), (103), (112), (201), (004), and (202) planes of wurtzite phase ZnO (JCPDS file No. 74-534). The predominant (002) and (004) peaks suggest that the ZnO nanorods grew with their *c*-axis orientation normal to the ITO surface. After electrodeposition of CdTe, three new peaks are observed in addition to the diffraction peaks from the hexagonal ZnO nanorods. These three broad peaks are centered at 23.96, 39.40, and 46.53°, which can be indexed respectively to the (111), (220), and (311) planes of the zinc-blende (ZB) CdTe (JCPDS file No. 65-880). After being annealed at 350 °C for 1 h, the crystallinity of CdTe

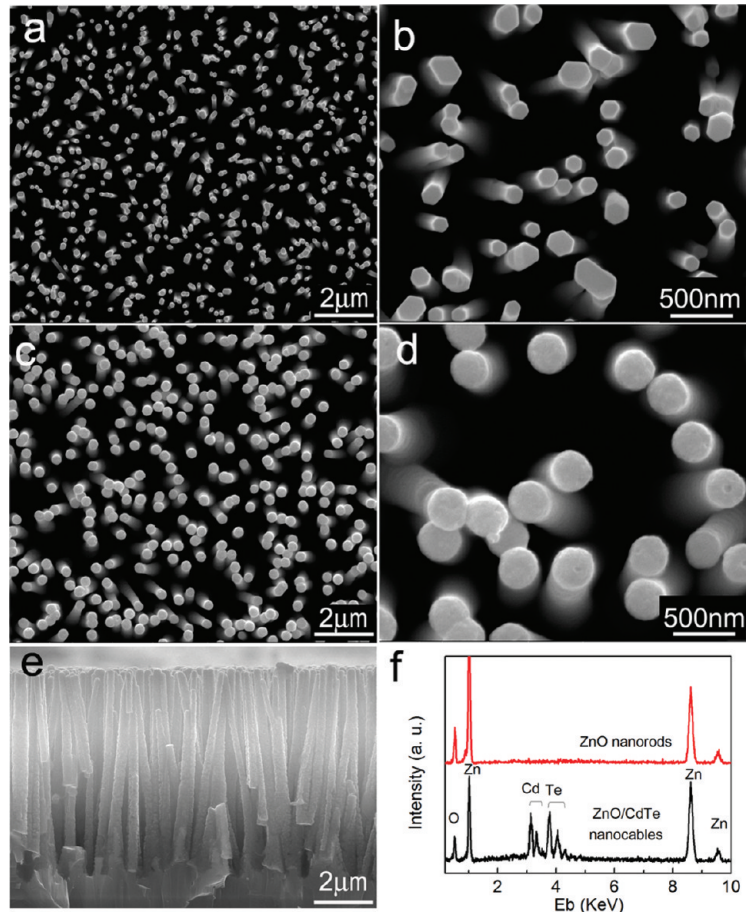

Figure 2. Top-view SEM images of ZnO nanorod arrays (a and b) and ZnO/CdTe nanocable arrays-on-ITO fabricated by the electrodeposition (c and d) at different magnifications. Panel e shows the cross-sectional SEM image of the ZnO/CdTe nanocable arrays-on-ITO, and panel f shows the EDX spectra of the ZnO nanorod arrays and ZnO/CdTe nanocable arrays.

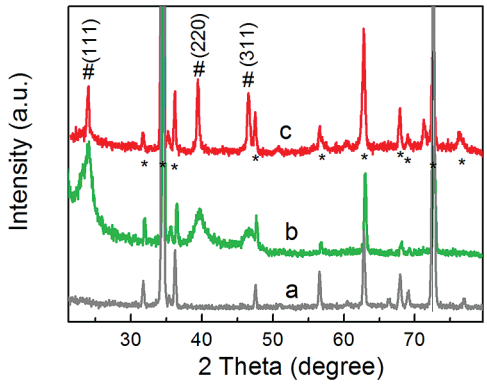

Figure 3. XRD patterns of the (a) ZnO nanorod arrays and (b) as-deposited and (c) postannealed ZnO/CdTe nanocable arrays-on-ITO.

shells is greatly enhanced, as suggested by the sharpening of the corresponding XRD peaks. Although intentional oxygen purging of the electrolyte before or during the electrodeposition process was not performed, diffraction peaks from oxide phases such as CdO or TeO_2 have not been detected.

By adjusting the total charge passed through the working electrode during the electrochemical deposition process, the thickness of the CdTe shell can be tuned from several tens to hundreds of nanometers. Figure 4 shows ZnO/CdTe nanocable arrays fabricated with different amounts of total charge. When the amount of the charge is increased to 6.7 C (Figure 4a,b), the CdTe shell thickness reaches ~160 nm, with a standard deviation of 20 nm. Reducing the amount of total charge to 0.7 C (Figure 4c,d) results in a CdTe shell thickness of only ~11 nm (standard deviation of 4 nm), while complete coverage of the ZnO core is still maintained.

The detailed microstructure of the ZnO/CdTe nanocable is further investigated by transmission electron microscopy (TEM)-related techniques. Figure 5a shows a low-magnification TEM image of a single ZnO/CdTe nanocable obtained by electrodeposition at 0.7 C total charge. Core−shell contrast can be clearly observed in this image. The core diameter is ~64 nm, while the shell thickness is ~11 nm. The EDX spectrum confirms that the nanocable is composed of Zn, O, Cd, and Te and that both the Zn/O and Cd/Te ratios are close to 1. The spatial distribution of the compositional elements within the nanocable is obtained using scanning transmission electron microscope (STEM)-EDX line scans along the nanocable's radial direction (marked by the red arrow in Figure 5a). In the intensity profile of the compositional elements shown in Figure 5b, the Zn and

O signals are mainly confined within the nanocable core area, while a higher intensity of Cd and Te is found in the shell region. This is consistent with the ZnO-core/CdTe-shell nanocable configuration observed in the TEM image. The ZnO core has a single-crystal wurtzite structure, which can be seen in the high resolution image taken from the same nanocable (Figure 5c). The CdTe shell appears to be polycrystalline with a ZB structure. Complete coverage of the ZnO core by the CdTe shell is realized without any interfacial void formation. The selective area electron diffraction (SAED) pattern (Figure 5d) taken from the same nanocable contains one set of diffraction spots that can be indexed to the [100] zone axis of the hexagonal ZnO, and several diffraction rings that can be indexed to ZB CdTe (111), (220), and (311) planes. The obvious diffraction spots within these diffraction rings suggest reasonable crystallinity of the CdTe grains in the continuous, polycrystalline shell. The HRTEM image of the nanocable's tip (Figure 5e) shows that the top surface of the ZnO nanorod has been also capped with CdTe. One may notice that in all of the ZnO/CdTe nanocable samples, the bare ZnO nanowires or nanorods have hexagonal structure with *c*-axis perpendicular to substrate surface, namely, the top surface at the tip of the ZnO nanowire is {0001} plane, and the side planes belong to {1$\bar{1}$00} planes. This explains the hexagonal cross section of the bare ZnO nanowire. As a comparison, the CdTe nanoshells were composed of many crystals with random orientations to the ZnO core. To minimize the surface energy of the nanocable, one shall expect a cylindrical surface without specific facet, which explains the circle-like cross section of the nanocable.

Figure 6 shows typical absorption spectra of the pure ZnO nanorods and of the postannealed ZnO/CdTe nanocable arrays (CdTe shell thickness of 88 ± 10 nm) on an ITO substrate. For the pure ZnO nanorod array, a steep UV absorption edge occurs at ~3.2 eV, consistent with the band gap of ZnO. A red shift of the absorption edge to ~1.5 eV is observed for the annealed ZnO/CdTe nanocable arrays on an ITO substrate, corresponding well with the band gap of CdTe.[30]

Figure 7 shows the photoluminescence (PL) spectra of the pure ZnO nanorod array (plot a) and the annealed ZnO/CdTe nanocable array with shell thickness of ~88 nm (plot b). For the bare ZnO nanorod array, a strong near-band-edge (NBE) emission can be clearly found at ~3.23 eV with negligible emission peaks associated with deep-level defects, despite the large surface area of the ZnO nanorods. After CdTe shell deposition, significant quenching of the ZnO NBE peak is observed. In addition, the NBE emission of CdTe (inset, plot d) is also largely depressed compared to that of the electrodeposited CdTe thin films (inset, plot c). The drastic quenching of the NBE emissions for both ZnO and CdTe in the nanocable configuration is reasonable, considering the band alignment between ZnO and

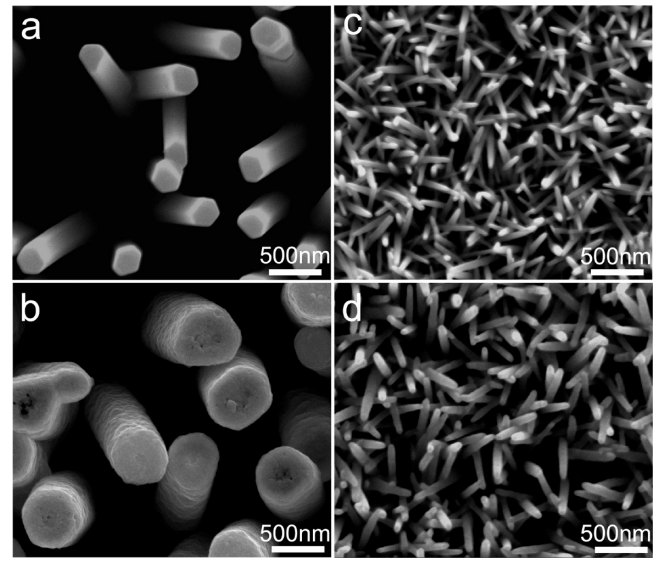

Figure 4. ZnO nanorod arrays (a) before and (b) after electrodeposition with total charge of 6.7 C; ZnO nanorod arrays (c) before and (d) after electrodeposition with total charge of 0.7 C.

CdTe, since a typical type II band alignment would enable the separation of photogenerated charge carriers, and thus reduce the electron−hole recombination

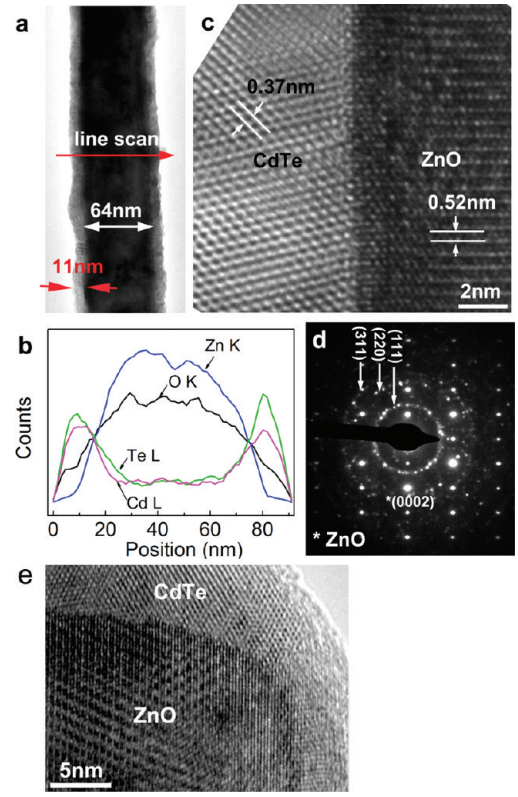

Figure 5. (a) Low-magnification TEM image showing the uniform morphology of a single ZnO/CdTe nanocable; (b) elemental profile extract from a STEM-EDX showing the distribution of the compositional elements (Zn, O, Te, and Cd) along the radial direction of the nanocable (indicated by the red arrow in panel a); (c, d) typical HRTEM image and SAED taken from the same ZnO/CdTe nanocable, showing the interface and crystalline structure of the nanocable. (e) HRTEM image taken from the tip of the ZnO/CdTe nanocable.

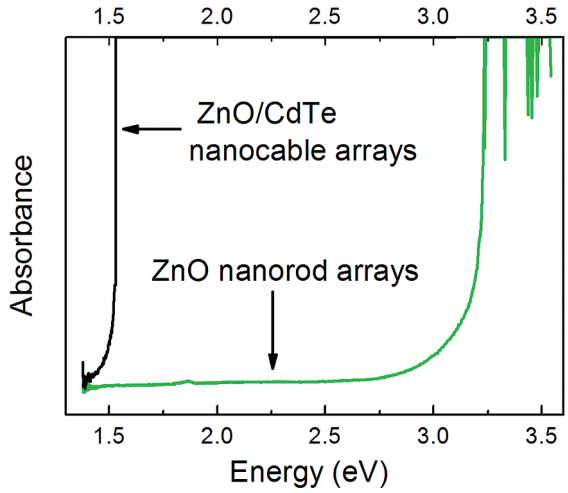

Figure 6. Absorption spectra of the ZnO nanorod arrays and postannealed ZnO/CdTe nanocable arrays on an ITO substrate.

probability within both ZnO and CdTe.[37−39] We have also carried out a series of ZnO PL emissions at different CdTe shell thicknesses (*i.e.*, shell thickness ~11 and 160 nm, see Supporting Information Figure 1a,b), and no significant difference can be found in the ZnO PL emission—quenching of the ZnO band edge is always observed. Similar results are obtained in the PL of CdTe (see Supporting Information Figure 1c,d). These results also suggest that charge carrier separation as driven by the proper band alignment between ZnO and CdTe serves as the major contributor to the observed ZnO and CdTe PL quenching, while interfacial recombination, depletion, and photon blocking (by thick surface layer) have little contributions.

The absorption properties of CdTe and the type II band alignment between CdTe and ZnO should lead to good photovoltaic performance of the nanocable array. This has been observed experimentally by using the ZnO/CdTe nanocable arrays-on-ITO as a photoelectrode. Figure 8 shows the current density *versus* potential (*J*−*V*) curves for the annealed ZnO/CdTe nanocable arrays measured both in the dark and under illumination. In the dark, the *J*−*V* curve shows typical rectifying behavior, with a weak current density of ~0.2 mA/cm^2 at a potential of 0 V. The large photocurrent density of ~5.9 mA/cm^2 is observed with zero bias potential (*vs* SCE) when the photoelectrode is illuminated by visible light. This represents more than a 30-fold increase in the current density over the measurement performed in the dark. The corresponding photocurrent response to ON−OFF cycling is shown in the inset of Figure 8, from which one can see that steady and prompt photocurrent generation can be obtained during on and off cycles of illumination. Compared with recently reported photocurrent densities for photoelectrodes that are similar, except for the use of CdTe QDs as the light harvester, usually less than 1 mA/cm^2,[25,26] our results suggest that vertically aligned ZnO/CdTe nanocable array photoelectrodes have superior photoelectrochemical properties. It is believed that the dense CdTe shell and high-quality CdTe/ZnO interface

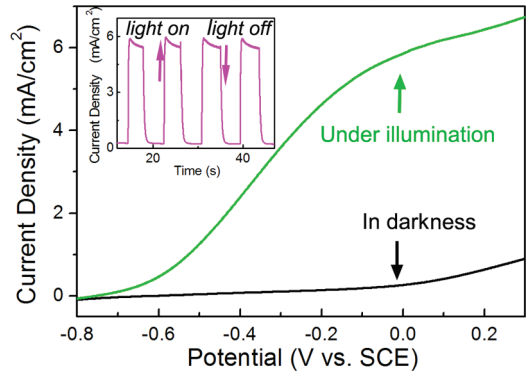

Figure 8. Current density *versus* potential curves for the ZnO/CdTe nanocable arrays-on-ITO photoelectrode measured in the dark and under an illumination of AM 1.5 light at 100 mW/cm^2. The inset shows the photocurrent response to ON−OFF cycles of AM 1.5 illumination at a constant potential of 0 V *vs* SCE.

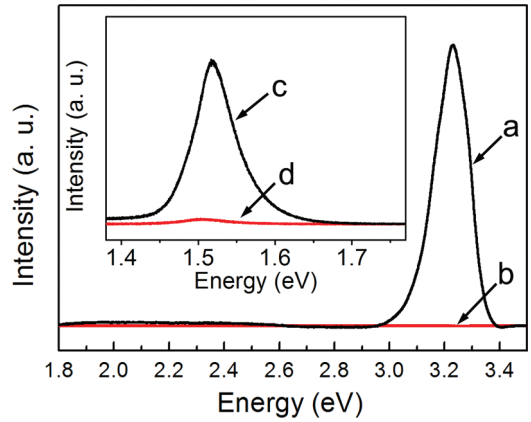

Figure 7. Room-temperature PL spectra: ZnO NBE emission in (a) ZnO nanorods and (b) ZnO/CdTe nanocables; CdTe NBE emission in (c) pure CdTe films and (d) ZnO/CdTe nanocables.

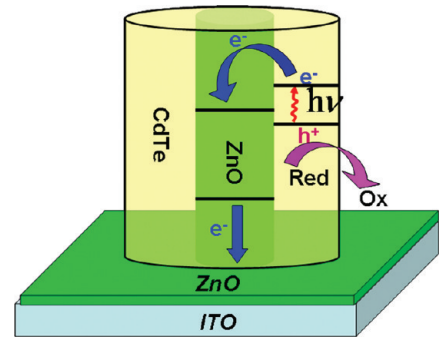

Figure 9. Schematic of the operation of the semiconductor sensitized solar cell: Electron injection from excited CdTe nanocrystal shell into ZnO nanorod core and scavenging of holes by a S^{2-}/Sn^{2-} red−ox couple. The vertically aligned nanocable architecture provides a direct pathway for electron transport from ZnO to the ITO substrate. The energy levels of VBM and CBM for both ZnO and CdTe are given as reference.[32]

greatly enhance absorption in the visible light range and favor charge separation, which together result in the impressive photocurrent measured.

The type II band alignment between ZnO and CdTe and the nanocable array configuration are the two most significant factors contributing to the observed photoelectrochemical behavior. As shown by the energy diagram in the schematic of the ZnO/CdTe nanocable photoelectrode (Figure 9), both the valence-band maximum (VBM) and conduction-band minimum (CBM) of CdTe lie above those of ZnO, with a conduction-band offset of ~1.02 eV.[32] In such a configuration, the photogenerated electrons can be easily injected from the CdTe shell into the ZnO nanorod core, driven by the band alignment, and then transported to the ITO substrate along the single-crystal ZnO, which provides a direct path for electron transport.

CONCLUSIONS

Fabrication of a large-scale, vertically aligned ZnO/CdTe nanocable array-on-ITO has been demonstrated using simple electrochemical deposition in a close-to-neutral electrolyte. The high crystallinity of both CdTe and ZnO, the type II band alignment between the two materials, the favorable absorption properties of CdTe, and the aligned nanocable configuration contribute to the good photovoltaic performance of this photoelectrode. The close-to-neutral electrochemical deposition method provides a general route for plating CdTe onto various semiconductor nanostructures.

METHODS

ZnO/CdTe Nanocable Array Preparation. A two-step method was adopted to fabricate ZnO/CdTe nanocable arrays. First, the ZnO nanorod array, on which the CdTe shell will be deposited, is prepared on an ITO substrate (20 Ω/□) using a conventional thermal evaporation method.[40] The electrodeposition of the CdTe shell is then carried out in an electrochemical workstation (CH Instrument, model 600B) with a three-electrode system. The ZnO nanorod array-on-ITO, a standard SCE, and Pt foil were used as the working electrode, the reference electrode, and the counter-electrode, respectively. The electrolyte was an aqueous solution of 0.005 M potassium tellurite (K_2TeO_3), 0.05 M nitrilotriacetic acid trisodium salt (NTA, $C_6H_6NO_6Na_3$), and 0.02 M cadmium acetate ($CdC_4H_6O_4$), with a solution pH of 8.3. K_2TeO_3 was synthesized *via* the reaction of TeO_2 powder (5 N) and hot KOH solution (70 °C), with a TeO_2/KOH molar ratio of 1:2, under vigorous magnetic stirring for 3 h. The electrodeposition of CdTe was performed at a fixed potential of −1.0 V *versus* SCE. The duration of the deposition process and the total charge passed through the electrodes were both varied. Fabricated nanocable array samples were then annealed at 350 °C for 1 h in an Ar atmosphere.

Structural, Optical, and Photoelectrochemical Property Characterization. The microstructure and crystallinity of the samples were examined using field-emission scanning electron microscopy (FE-SEM, FEI Quautum F400), scanning transmission electron microscopy (STEM, TEM, Tecnai 20, FEG, equipped with an energy dispersive X-ray (EDX) spectrometer), and X-ray diffraction (XRD, Ragiku RU300). The optical properties were investigated by photoluminescence (PL) and absorption measurements (UV−vis−IR spectrometer, U3501) performed at room temperature. For the PL measurements, the 325 nm line of a HeCd laser and the 514 nm line of an argon laser were applied to ZnO and CdTe, respectively. Photoelectrochemical measurements were performed in a sulfide/polysulfide (S^{2-}/Sn^{2-}) electrolyte containing 0.5 M S and 0.3 M Na_2S dissolved in deionized water, during which the ZnO/CdTe nanocable arrays on ITO, Pt foil, and SCE were used as the working electrode, the counter-electrode, and the reference electrode, respectively. An AM 1.5 G light with a power of 100 mW/cm^2 was used as the illumination source. Photocurrent on and off cycles were measured using the same electrochemical workstation and the same illumination source.

Acknowledgment. This work was supported by grants from the GRF of HKSAR under project No. 414908, CUHK Focused Investment Scheme C, CUHK Group Research Scheme, NSFC No. 50772032, and NSF of Hubei Province No. 2009CDA035.

Supporting Information Available: Room-temperature PL spectra of ZnO NBE emission in ZnO/CdTe nanocable arrays. This material is available free of charge *via* the Internet at http://pubs.acs.org.

REFERENCES AND NOTES

1. Oregan, B.; Grätzel, M. A. Low-Cost, High-Efficiency Solar-Cell Based on Dye-Sensitized Colloidal TiO_2 Films. *Nature* **1991**, *353*, 737–740.
2. Chang, C. H.; Lee, Y. L. Chemical Bath Deposition of CdS Quantum Dots onto Mesoscopic TiO_2 Films for Application in Quantum-Dot-Sensitized Solar Cells. *Appl. Phys. Lett.* **2007**, *91*, 053503.
3. Robel, I.; Subramanian, V.; Kuno, M.; Kamat, P. V. Quantum Dot Solar Cells. Harvesting Light Energy with CdSe Nanocrystals Molecularly Linked to Mesoscopic TiO_2 Films. *J. Am. Chem. Soc.* **2006**, *128*, 2385–2393.
4. Shen, Q.; Kobayashi, J.; Diguna, L. J.; Toyoda, T. Effect of ZnS Coating on the Photovoltaic Properties of CdSe Quantum Dot-Sensitized Solar Cells. *J. Appl. Phys.* **2008**, *103*, 084304.
5. Niitsoo, O.; Sarkar, S. K.; Pejoux, C.; Ruhle, S.; Cahen, D.; Hodes, G. Chemical Bath Deposited CdS/CdSe-Sensitized Porous TiO_2 Solar Cells. *J. Photochem. Photobiol. A* **2006**, *181*, 306–313.
6. Plass, R.; Serge, P.; Kruger, J.; Grätzel, M.; Bach, U. Quantum Dot Sensitization of Organic−Inorganic Hybrid Solar Cells. *J. Phys. Chem. B* **2002**, *106*, 7578–7580.
7. Hoyer, P.; Könenkamp, R. Photoconduction in Porous TiO_2 Sensitized by PbS Quantum Dots. *Appl. Phys. Lett.* **1995**, *66*, 349–351.
8. Schaller, R. D.; Klimov, V. I. High Efficiency Carrier Multiplication in PbSe Nanocrystals: Implications for Solar Energy Conversion. *Phys. Rev. Lett.* **2004**, *92*, 186601.
9. Zaban, A.; Mićić, O. I.; Gregg, B. A.; Nozik, A. J. Photosensitization of Nanoporous TiO_2 Electrodes with InP Quantum Dots. *Langmuir* **1998**, *14*, 3153–3156.
10. Yu, P. R.; Zhu, K.; Norman, A. G.; Ferrere, S.; Frank, A. J.; Nozik, A. J. Nanocrystalline TiO_2 Solar Cells Sensitized with InAs Quantum Dots. *J. Phys. Chem. B* **2006**, *110*, 25451–25454.
11. Alivisatos, A. P. Semiconductor Clusters, Nanocrystals, and Quantum Dots. *Science* **1996**, *271*, 933–937.
12. Robel, I.; Kuno, M.; Kamat, P. V. Size-Dependent Electron Injection from Excited CdSe Quantum Dots into TiO_2 Nanoparticles. *J. Am. Chem. Soc.* **2007**, *129*, 4136–4137.
13. López-Luke, T.; Wolcott, A.; Xu, L. P.; Chen, S. W.; Wen, Z. H.; Li, J. H.; De La Rosa, E.; Zhang, J. Z. Nitrogen-Doped and CdSe Quantum-Dot-Sensitized Nanocrystalline TiO_2 Films for Solar Energy Conversion Applications. *J. Phys. Chem. C* **2008**, *112*, 1282–1292.

14. Carlson, B.; Leschkies, K.; Aydil, E. S.; Zhu, X. Y. Valence Band Alignment at Cadmium Selenide Quantum Dot and Zinc Oxide (10−10) Interfaces. *J. Phys. Chem. C* **2008**, *112*, 8419–8423.
15. Kuang, D.; Brillet, J.; Chen, P.; Takata, M.; Uchida, S.; Miura, H.; Sumioka, K.; Zakeeruddin, S. M.; Grätzel, M. Application of Highly Ordered TiO_2 Nanotube Arrays in Flexible Dye-Sensitized Solar Cells. *ACS Nano* **2008**, *2*, 1113–1116.
16. Martinson, A. B. F.; Elam, J. W.; Hupp, J. T.; Pellin, M. J. ZnO Nanotube Based Dye-Sensitized Solar Cells. *Nano Lett.* **2007**, *7*, 2183–2187.
17. Kang, T. S.; Smith, A. P.; Taylor, B. E.; Durstock, M. F. Fabrication of Highly-Ordered TiO_2 Nanotube Arrays and Their Use in Dye-Sensitized Solar Cells. *Nano Lett.* **2009**, *9*, 601–606.
18. Ku, C. H.; Wu, J. J. Electron Transport Properties in ZnO Nanowire Array/Nanoparticle Composite Dye-Sensitized Solar Cells. *Appl. Phys. Lett.* **2007**, *91*, 093117.
19. Shankar, K.; Bandara, J.; Paulose, M.; Wietasch, H.; Varghese, O. M.; Mor, G. K.; LaTempa, T. J.; Thelakkat, M.; Grimes, C. A. Highly Efficient Solar Cells Using TiO_2 Nanotube Arrays Sensitized with a Donor-Antenna Dye. *Nano Lett.* **2008**, *8*, 1654–1659.
20. Leschkies, K. S.; Divakar, R.; Basu, J.; Enache-Pommer, E.; Boercker, J. E.; Carter, C. B.; Kortshagen, U. R.; Norris, D. J.; Aydil, E. S. Photosensitization of ZnO Nanowires with CdSe Quantum Dots for Photovoltaic Devices. *Nano Lett.* **2007**, *7*, 1793–1798.
21. Sun, W. T.; Yu, Y.; Pan, H. Y.; Gao, X. F.; Chen, Q.; Peng, L. M. CdS Quantum Dots Sensitized TiO_2 Nanotube-Array Photoelectrodes. *J. Am. Chem. Soc.* **2008**, *130*, 1124–1125.
22. Kongkanaed, A.; Tvrdy, K.; Takechi, K.; Kuno, M.; Kamat, P. V. Quantum Dot Solar Cells. Tuning Photoresponse through Size and Shape Control of CdSe−TiO_2 Architecture. *J. Am. Chem. Soc.* **2008**, *130*, 4007–4015.
23. Lee, W.; Kang, S. H.; Kim, J.-Y.; Kolekar, G. B.; Sung, Y.-E.; Han, S. H. TiO_2 Nanotubes with a ZnO Thin Energy Barrier for Improved Current Efficiency of CdSe-Quantum Dot-Sensitized Solar Cells. *Nanotechnology* **2009**, *20*, 335706.
24. Baker, D. R.; Kamat, P. V. Photosensitization of TiO_2 Nanostructures with CdS Quantum Dots: Particulate *versus* Tubular Support Architectures. *Adv. Funct. Mater.* **2009**, *19*, 805–811.
25. Cao, X. B.; Chen, P.; Guo, Y. Decoration of Textured ZnO Nanowires Array with CdTe Quantum Dots: Enhanced Light-Trapping Effect and Photogenerated Charge Separation. *J. Phys. Chem. C* **2008**, *112*, 20560–20566.
26. Seabold, J. A.; Shankar, K.; Wilke, R. H. T.; Paulose, M.; Varghese, O. K.; Grimes, C. A.; Choi, K. S. Photoelectrochemical Properties of Heterojunction CdTe/TiO_2 Nanotube Arrays. *Chem. Mater.* **2008**, *20*, 5266–5273.
27. Lee, H. J.; Yum, J. H.; Leventis, H. C.; Zakeeruddin, S. M.; Haque, S. A.; Chen, P.; Seok, S. I.; Grätzel, M.; Nazeeruddin, M. K. CdSe Quantum Dot-Sensitized Solar Cells Exceeding Efficiency 1% at Full-Sun Intensity. *J. Phys. Chem. C* **2008**, *112*, 11600–11608.
28. Kamat, P. V. Quantum Dot Solar Cells. Semiconductor Nanocrystals as Light Harvesters. *J. Phys. Chem. C* **2008**, *112*, 18737–18753.
29. Hodes, G. Comparison of Dye- and Semiconductor-Sensitized Porous Nanocrystalline Liquid Junction Solar Cells. *J. Phys. Chem. C* **2008**, *112*, 17778–17787.
30. Shokhovets, S.; Ambacher, O.; Gobsch, G. Conduction-Band Dispersion Relation and Electron Effective Mass in III−V and II−VI Zinc-Blende Semiconductors. *Phys. Rev. B* **2007**, *76*, 125203.
31. Breeze, A. J. Next Generation Thin-Film Solar Cells. *Proc. 46th Ann. 2008 IEEE Int. Reliabil. Phys. Symp.* **2008**, 168–171.
32. Van de Walle, C. G.; Neugebauer, J. Universal Alignment of Hydrogen Levels in Semiconductors, Insulators, and Solutions. *Nature* **2003**, *423*, 626–628.
33. Kum, M. C.; Yoo, Y. B.; Rheem, Y. W.; Bozhilov, K. N.; Chen, W.; Mulchandani, A.; Myung, N. M. Synthesis and Characterization of Cadmium Telluride Nanowire. *Nanotechnology* **2008**, *19*, 325711.
34. Zhao, A. W.; Meng, G. W.; Zhang, L. D.; Gao, T.; Sun, S. H.; Pang, Y. T. Electrochemical Synthesis of Ordered CdTe Nanowire Arrays. *Appl. Phys. A: Mater. Sci. Process.* **2003**, *76*, 537–539.
35. Xu, D. S.; Guo, Y. G.; Yu, D. P.; Guo, G. L.; Tang, Y. Q.; Y, D. P. Highly Ordered and Well-Oriented Single-Crystal CdTe Nanowire Arrays by Direct-Current Electrodeposition. *J. Mater. Res.* **2002**, *17*, 1711–1714.
36. Dergacheva, M. B.; Statsyuk, V. N.; Fogel, L. A. Electrodeposition of CdTe from Ammonia-Chloride Buffer Electrolytes. *J. Electroanal. Chem.* **2005**, *579*, 43–49.
37. Wang, K.; Chen, J. J.; Zhou, W. L.; Zhang, Y.; Yan, Y. F.; Pern, J.; Mascarenhas, A. Direct Growth of Highly Mismatched Type II ZnO/ZnSe Core/Shell Nanowire Arrays on Transparent Conducting Oxide Substrates for Solar Cell Applications. *Adv. Mater.* **2008**, *20*, 3248–3253.
38. Zhang, Y.; Wang, L. W.; Mascarenhas, A. Quantum Coaxial Cables for Solar Energy Harvesting. *Nano Lett.* **2007**, *7*, 1264–1269.
39. Kumar, S.; Jones, M.; Lo, S.; Scholes, G. Nanorod Heterostructures Showing Photoinduced Charge Separation. *Small* **2007**, *3*, 1633–1639.
40. Zhou, M. J.; Zhu, H. J.; Jiao, Y.; Rao, Y. Y.; Hark, S. K.; Liu, Y.; Peng, L. M.; Li, Q. Optical and Electrical Properties of Ga-Doped ZnO Nanowire Arrays on Conducting Substrates. *J. Phys. Chem. C* **2009**, *113*, 8945–8947.